RSC Advances

PAPER

View Article Online
View Journal | View Issue

Cite this: *RSC Adv.*, 2014, **4**, 47726

MnO_2-doped, polyaniline-grafted rice husk ash nanocomposites and their electrochemical capacitor applications†

P. Prabunathan, K. Sethuraman and M. Alagar*

Received 16th May 2014
Accepted 15th September 2014

DOI: 10.1039/c4ra04633a

www.rsc.org/advances

The utilization of renewable rice husk ash (RHA) in an energy storage system without any activation is described. Polyaniline-grafted RHA (PANI/RHA) and MnO_2-doped, polyaniline-grafted RHA (PANI/MnO_2/RHA) nanocomposites were developed. The capacitance behaviour of the developed nanocomposites was well studied using cyclic voltammetry and charge–discharge methods. The results of galvanostatic charging and discharging show a 17-fold improvement in capacitance behaviour of PANI/RHA and a 54-fold enhanced capacitance of PANI/MnO_2/RHA nanocomposites compared to that of neat RHA. The enhanced capacitance and rate capability of RHA are attributed to the synergistic effect of polyaniline with RHA and also the high utilization of pseudo-active species for ion/electron transfer.

Introduction

In recent years, the natural environment has been gradually endangered by the diversity of hazardous materials released from man-made products and waste from biomass sources.[1] Similarly, increasing demands for fossil fuel energy and an increasing awareness of sustainability issues have given rise to the use of biomass for energy generation as well as storage applications, which helps to reduce the use of environmentally hazardous materials.[2] Materials such as carbon, carbon-based composites with conductive polymers (polyaniline, polypyrrole) and pseudo-capacitive materials (RuO_2, MnO_2 and CeO_2) are well-known super capacitor anode materials. Their synergistic effects towards capacitor performance are well described.[3–8] Activated carbon from bio-sources has been reported in research efforts towards the proper usage of renewable materials in storage applications. However, the synthesis of activated carbon involves less economical, multistep pathways and utilizes activating agents ($ZnCl_2$, H_3PO_3, *etc.*).[9–12]

One of the major naturally occurring bio-resources is rice husk ash (RHA), which is the most abundant agricultural residue from agriculture-based countries. RHA has been utilized in a wide range of applications and in different forms. The major constituents of rice husk are silica (SiO_2), at about 60%, and carbon (C), ranging from 10 to 40%. The silica derived from rice husk ash (RHA) has been used as a catalyst support,[13] adsorbent,[14] and composite.[15] Similarly, RHA has been used as an electrode material and an electrical capacitor.[16–18] Thus, the crystalline, nanosized silicon derived from the rice husk ash has been used as a promising anode material for Li ion batteries,[19,20] and the activated carbon from rice husk ash has also been utilized as a capacitor anode material.[21,22] Rice husk is constituted by silica, exhibiting an insulating behavior, and a carbonaceous material, which contributes to the conductive behavior. Thus, the insulating behavior of RHA can be exploited by compositing the materials with conducting substrates and using it in energy storage systems. Likewise, it has been reported that the use of silica core offers high colloidal stability and easily controllable particle size.[2]

The present work highlights the performance of naturally available RHA bio-source in the fabrication of super capacitor anode materials. Similarly, the sustainable RHA was composited with MnO_2 doping and polyaniline grafting, without an activation step. Grafting of polyaniline over the RHA was primarily ascertained with FT-IR and CP-MAS. Further doping of MnO_2 on the RHA was supported by XPS and analytical characterization methods, such as HR-SEM/EDAX and HR-TEM analysis. Electrochemical studies of PANI/RHA and PANI/MnO_2/RHA composites suggest that the developed nanocomposites are highly suitable towards the fabrication of supercapacitor anodes without utilizing any activation process.

Experimental section

Materials

Manganese sulphate (≥99.8%) was obtained from Alfa Aesar. Aniline (monomer), ammonium persulphate, potassium permanganate, sodium sulfate and hydrochloric acid were obtained from Merck, India, and double distilled water was used throughout the work.

Polymer Composite Lab, Department of Chemical Engineering, Anna University, Chennai, 600 025, Tamilnadu, India. E-mail: mkalagar@yahoo.com; Fax: +91 4422359164; Tel: +91 4422359164

† Electronic supplementary information (ESI) available. See DOI: 10.1039/c4ra04633a

Step 1: synthesis of rice husk ash (RHA)

The rice husk was collected from the local agriculture waste facility, and it was synthesized as per the previously reported procedure.[23] Initially, rice husk was washed with distilled water and dried in hot air oven at approximately 60 °C for 8 h. It was then washed with acetone followed by HCl (0.3 M) to remove other contaminants and subsequently dried in hot air oven at approximately 60 °C for 8 h. Finally, the rice husk was placed in a muffle furnace for 6 h at 350 °C in order to obtain pure rice husk ash (RHA). The compositions of the resulting products are given in the supporting information (Fig. S1b and Table S3†). For comparison, the composition of raw rice husk ash is also given (Fig. S1a, ESI†).

Step 2: synthesis of polyaniline-grafted rice husk ash (PANI/RHA)

The grafting of highly conductive polyaniline over rice husk ash (PANI/RHA) was developed as per the reported procedure.[24] 1 g of rice husk ash and 1 mL of freshly distilled aniline monomer were added to 50 mL of 1 M HCl and subsequently sonicated for 30 minutes. Then, the required amount of homogeneous solution containing ammonium persulphate dissolved in 50 mL of hydrochloric acid (1 M) was slowly added with simultaneous efficient agitation for 5 h at 0–5 °C in an ice bath. Then, the product was filtered, subsequently washed several times with 1 M HCl and finally in deionized water to separate the impurities. The resulting product was then dried in a hot air oven at 60 °C for 12 h.

Step 3: synthesis of polyaniline-grafted, MnO_2-doped rice husk ash PANI/MnO_2/RHA nanocomposites

RHA prepared in Step 1 was dispersed in acidified water (pH = 2); then, the desired amount of $MnSO_4 \cdot H_2O$ (0.1 M) was added and subjected to ultra-sonication for 1 h. Then, an equivalent amount of $KMnO_4$ (0.05 M) dissolved in water (pH = 2) was added slowly under continuous sonication for 3 h. Subsequent stirring of the mixture overnight yielded MnO_2-doped RHA (MnO_2/RHA). The resulting product was centrifuged with repeated washing. After drying, the same was utilized to graft polyaniline by repeating the abovementioned procedure (Step 2).

Characterization

FT-IR spectral data were obtained using a Perkin Elmer 6X FT-IR spectrometer. The solid-state NMR of raw RHA and RHA/polyaniline were analyzed at 14.1 and 11.7 T, respectively, on a Bruker DRX-500 spectrometer equipped with 4 mm MAS probes. Thermogravimetric analysis (TGA) was performed on a Netzsch STA 409 thermogravimetric analyzer. A Hitachi S-4800 high resolution-scanning electron microscope (HR-SEM) equipped with Horiba was used to record the morphology, with the composition at 20 kV. HRTEM images were captured using a TECNAI G_2 S-Twin transmission electron microscope with an acceleration voltage of 150 kV. TEM samples were prepared by dispersing the composites in ethanol, mounting them on carbon-coated Cu TEM grids, and drying for 24 h at 30 °C to obtain a film of <100 nm in size. Powder X-ray diffraction patterns (XRD) were recorded using a Rigaku Miniflex diffractometer with Cu-KR radiation (k = 0.154 nm). The diffraction data was recorded in the 2θ over the range of 5–80°. XPS was measured using an Omicron nanotechnology instrument at a pressure below 10^{-10} Torr. The wide scan was used to record the core level of atoms with a monochromatic Al-Kα radiation (photon energy 1/4 1486.6 eV) at a pass energy of 15 V and electron take-off angle of 60°.

The electrochemical measurements were carried out in a CHI660D electrochemical workstation. A three-electrode assembly was equipped with a working electrode, a platinum counter electrode and Ag/AgCl reference electrode. In the present work, fabrication of the working electrode was achieved by coating a paste of nanocomposites into a pre-cleaned nickel plate with a surface area of 1 cm^2. Without adding any carbon, 2 mg of the prepared nanocomposites were mixed with a few drops of DMF, coated over the plate and subsequently allowed to dry overnight at 90 °C. Thus, the obtained electrode was utilized as a working electrode. Sodium sulphate (0.5 M) was used as an electrolyte to analyze the performance of the working electrode. Cyclic voltammetry (CV), galvanostatic charge–discharge measurements and electrochemical impedance analysis were used to study the capacitance behavior of the nanocomposites. The specific capacitance of the nanocomposites was calculated from the discharge curve using the following formula:

$$C = \frac{I \times t}{m \times \Delta V} \quad (1)$$

Results and discussion

FT-IR spectra of RHA, PANI/RHA and PANI/MnO_2/RHA nanocomposites are presented in Fig. 1a–c. In Fig. 1a, the peaks at 1098, 799 and 465 cm^{-1} are due to Si–O–Si and Si–H vibrations in the RHA amorphous silica. The peak at 2924 cm^{-1} corresponds to the C–H group. The broad peak at around 3450 cm^{-1} corresponds to the presence of hydroxyl group in both water and Si–OH. The grafting of polyaniline over rice husk ash is illustrated in Scheme 1, and the corresponding vibrational spectrum is shown in Fig. 1b. The peaks at 1570 and 1476 cm^{-1} correspond to the typical C=C stretching vibration of the quinoid and benzenoid rings of polyaniline, whereas the peak at 1302 cm^{-1} is attributed to C–N stretching vibration.[24–27] Similar stretching modes were also observed in Fig. 1c, with an additional peak at 542 cm^{-1} representing the presence of MnO_2 in the nanocomposites; these are consistent with previously reported literature.[28]

The ^{13}C CP-MAS spectra of RHA and PANI/RHA are shown in Fig. 2a and b, respectively. The ^{13}C NMR signal at 29 ppm may be due to the presence of lignin or cellulose carbon, whereas the peak at 128 and 132 ppm corresponds to the aromatic carbon of cellulose. The ^{13}C NMR of PANI/RHA (Fig. 2b) was used to illustrate the presence of benzoid and quinoid aromatic carbons of

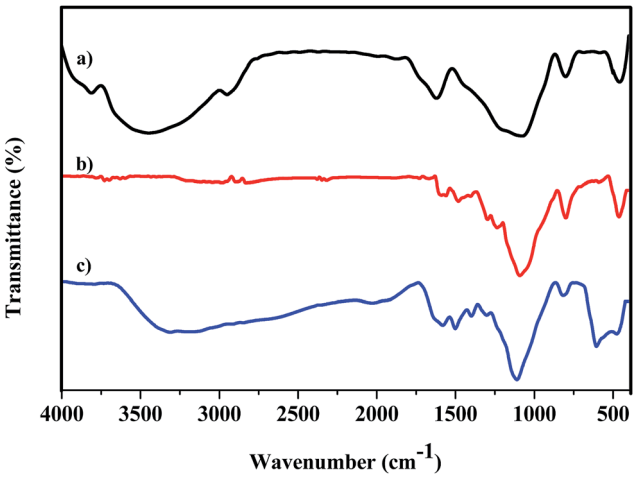

Fig. 1 FTIR spectra of (a) RHA, (b) PANI/RHA and (c) PANI/MnO_2/RHA nanocomposites.

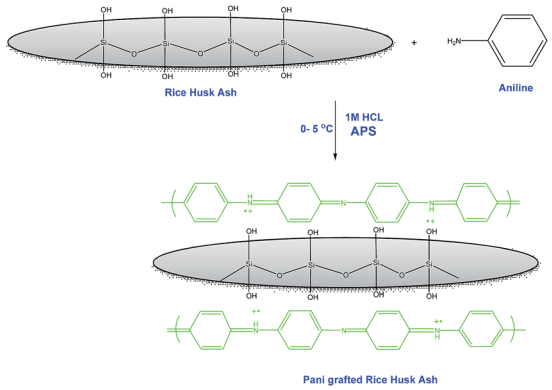

Scheme 1 Synthesis of polyaniline-grafted rice husk ash nanocomposite.

polyaniline, at 124.34 and 144.27 ppm, respectively. Further, the silica network of RHA and PANI/RHA was confirmed by ^{29}Si CP-MAS spectra, as shown in Fig. 2c and d, respectively. The RHA exhibits three well-defined characteristic peaks at −91, −99 and −109 ppm, which indicates the presence of Q^2 [geminal silanol, $(–SiO)_2Si(OH)_2$], Q^3 [single silanol, $(–SiO)_3–SiOH$] and Q^4 [siloxane, $(SiO)_4Si$] silicon atoms, respectively.

The peaks obtained for PANI/RHA at −99 and −109 ppm (Fig. 2c) indicate the existence of Q^3 and Q^4 silicon atoms, similar to those of neat RHA. The disappearance of the peak at −99 ppm is attributed to the structural changes in the Q^2 silicon atom (Fig. 2d) due to the interaction of RHA with polyaniline through weak van der Waals forces and hydrogen bonding.[29–34]

Further, the X-ray photoelectron survey spectrum presented in Fig. 3a confirms the grafting of polyaniline through the presence of N atom at 400 eV in addition to the Si, C, and O atoms in PANI/RHA nanocomposites. Additionally, the presence of Mn atom in the PANI/MnO_2/RHA nanocomposites was also ascertained from the peaks at 642.2 eV and 653.9 eV.

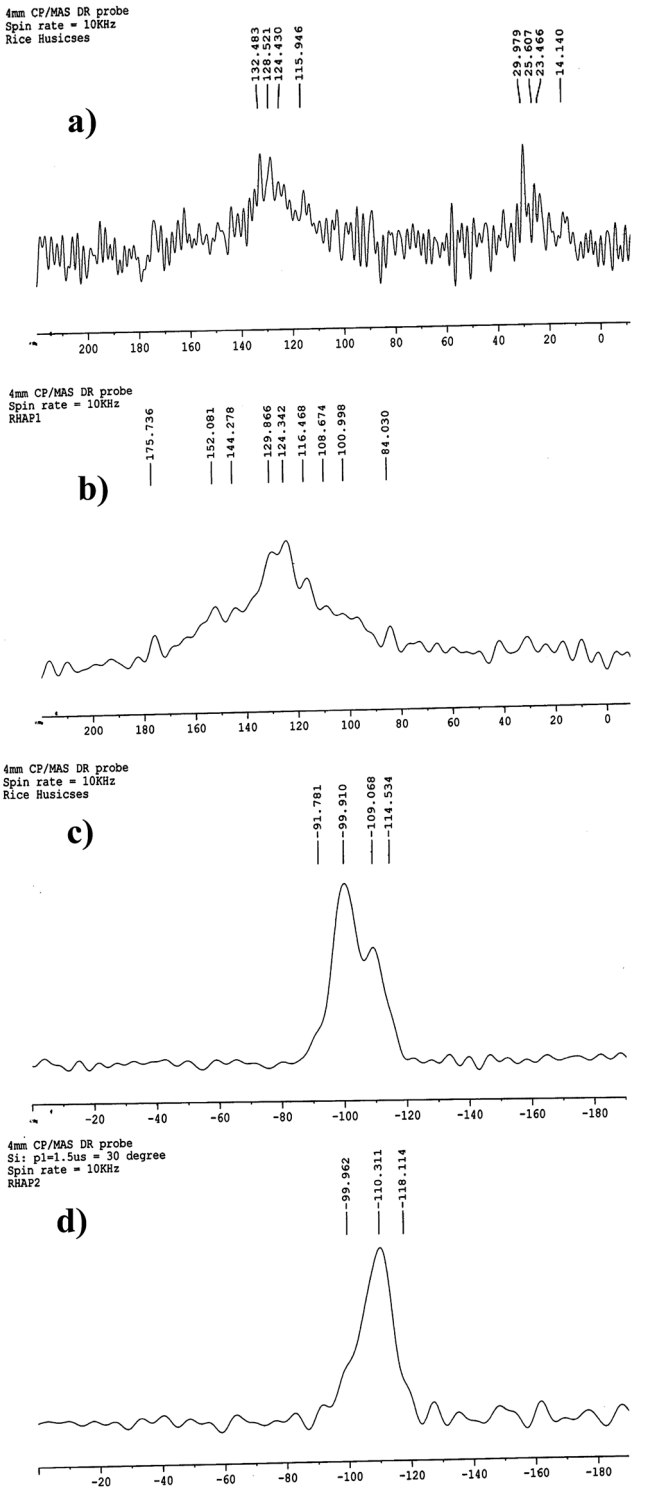

Fig. 2 Solid-state ^{13}C CP-MAS spectra of (a) RHA and (b) PANI/RHA; ^{29}Si CP-MAS spectra of (c) RHA and (d) PANI/RHA.

Fig. 3b illustrates the existence of Mn 2p3/2 and Mn 2p1/2, whose binding energies are 642.2 eV and 653.9 eV. These binding energy values confirm the presence of Mn^{4+} in the nanocomposites. Further, the spin energy separation of 11.7 eV

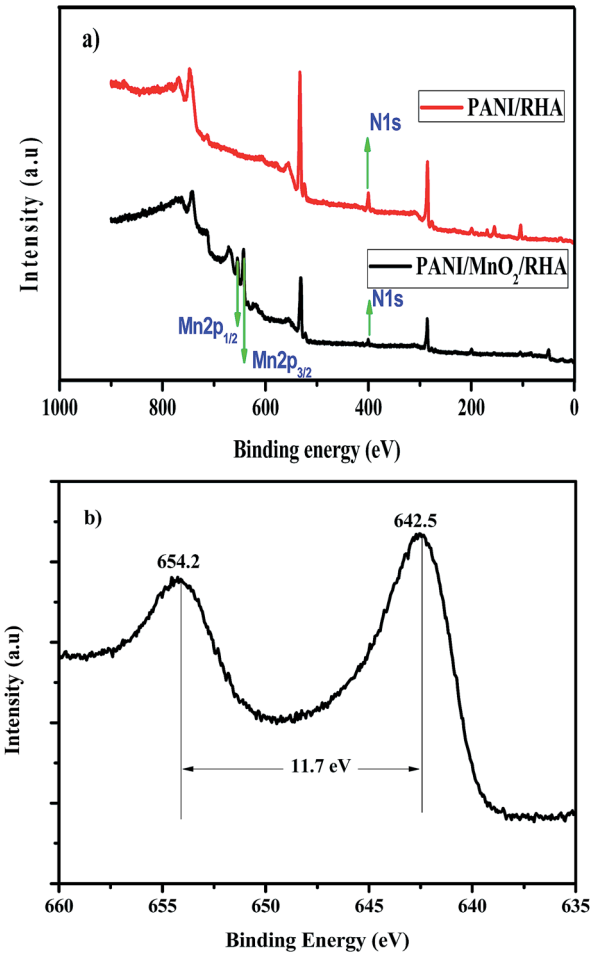

Fig. 3 XPS spectrum of (a) PANI/RHA, PANI/MnO_2/RHA nanocomposites and (b) manganese of PANI/MnO_2/RHA nanocomposites.

is also found to show good agreement with the reported data of Mn 2p3/2 and Mn 2p1/2 in MnO_2.[28]

The thermal stability of the RHA, PANI/RHA and PANI/MnO_2/RHA was analyzed using a thermogravimetric analyzer, and the thermograms are illustrated in Fig. 4. Three major regions of weight loss were observed in the thermograms of RHA, PANI/RHA and PANI/MnO_2/RHA. The initial-stage degradation observed below 200 °C may be attributed to the loss of water molecules physically adsorbed on the surface of the composites. Weight loss in the temperature range of 200–530 °C corresponds to the beginning of degradation of the polyaniline chain coated over the hybrid nanocomposites.[25] Weight loss above 530 °C indicates the complete degradation of polyaniline and the evolution of oxygen from MnO_2.[35] Among the three composites, PANI/MnO_2/RHA was found to be more stable up to 530 °C, due to its higher MnO_2 content.

Fig. 5 shows the N_2 adsorption and desorption isotherms of RHA, PANI/RHA and PANI/MnO_2/RHA. The rice husk ash shows 95 $m^2\ g^{-1}$ surface area with 0.20 $cm^3\ g^{-1}$ pore volume. Amorphous carbon and silica formed during burning are key factors for the surface area of rice husk ash upon burning at 350 °C. However, the fusion of particles at above 350 °C leads to partial

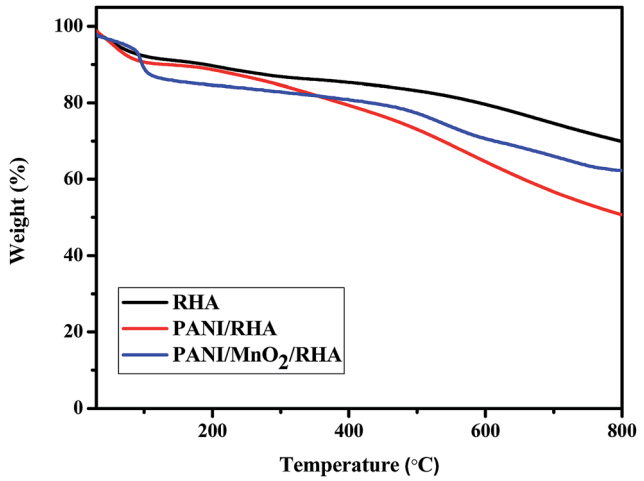

Fig. 4 TGA profile of RHA, PANI/RHA and PANI/MnO_2/RHA nanocomposites.

closure of pores and resulted in crystalline silica with lower surface area.[36,37]

Similarly, the N_2 adsorption and desorption isotherms of PANI/RHA and PANI/MnO_2/RHA suggest the presence of mesoporous nature in both nanocomposites with type IV hysteresis loops. However, PANI/MnO_2/RHA shows 558.7 $m^2\ g^{-1}$ surface area with 0.08 $cm^3\ g^{-1}$ pore volume, whereas PANI/RHA shows only 163 $m^2\ g^{-1}$ surface area with 0.19 $cm^3\ g^{-1}$ pore volume. The increased surface area of PANI/MnO_2/RHA may be attributed to the decreased particle size of the nanocomposites, and it has also been reported that the presence of MnO_2 can offer a higher surface area. Further, MnO_2 and polyaniline in the tertiary composites contribute to the enhanced surface area of the developed nanocomposites compared to the pristine material.[38–42] Further, the highly amorphous nature of the nanocomposites (Fig. 6) also contributes to the enhancement of surface area.

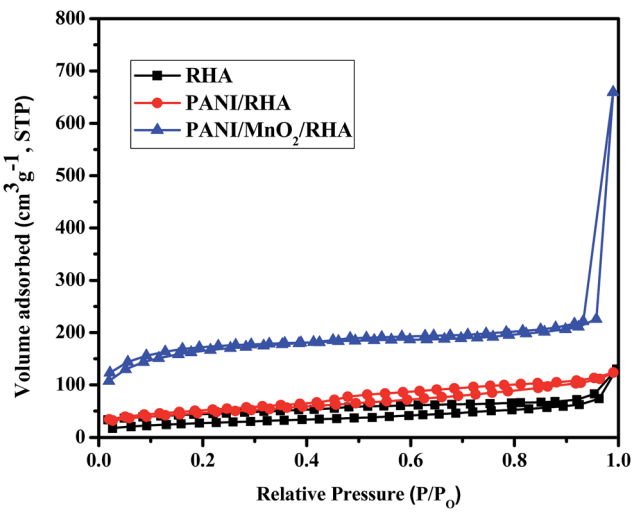

Fig. 5 BET profile of (a) RHA (b) PANI/RHA and (c) PANI/MnO_2/RHA nanocomposites.

The X-ray diffractogram of RHA, MnO_2, MnO_2/RHA, PANI/RHA and PANI/MnO_2/RHA are presented in Fig. 6. The broad reflection at 20° illustrates the amorphous nature of RHA (Fig. 6a). Similarly, the MnO_2-doped RHA also shows a broad reflection at 20°.[43] However, the lower intense broad peaks at 37.2° and 66.4° confirm the existence of MnO_2. The weak and broad signal of MnO_2 suggests the amorphous nature and is similar to previous reports.[44,45] The peaks at 9.5° and 25° in Fig. 6d confirm polyaniline grafting in the PANI/RHA nanocomposites. The reflection of PANI at 25° with *d*-spacing (~3.5 Å) corresponds to the face-to-face interchain stacking distance between phenyl rings.[2,46–49] It is noteworthy that no distinct MnO_2 reflection was observed in the tertiary PANI/MnO_2/RHA composite, indicating that the surface of the MnO_2/RHA has been homogenously and densely grafted with the polyaniline layer. Further, it was reported that polymerization of PANI disturbs the crystal structure of MnO_2 and thus leads to the formation of amorphous MnO_2.[50–52] Thus, the amorphous MnO_2 tunnel structures should be convenient for cation diffusion. Subsequently, this can render a large capacitance.[53]

The SEM micrographs of RHA, PANI/RHA, and PANI/MnO_2/RHA are illustrated in Fig. 7a–c. The grafting of polyaniline over RHA is achieved by surface polymerization, which also seems to be uniform and shows the compatibility of rice husk ash with polyaniline. The adhesion of polyaniline was achieved at not only the macroscopic level, but also at the mesopore level of the rice husk.[54]

Further, the fibrous appearance of PANI offers a higher surface area with improved porosity for both PANI/RHA and PANI/MnO_2/RHA nanocomposites. The same is supported by the N_2 adsorption studies, which gave a high surface area for PANI/RHA (Fig. 5).

It was also found that the MnO_2 nanoparticles are successfully and uniformly deposited over the surface of the RHA-like needle morphology, indicated by the arrow mark in the ESI (Fig. S5†).[55] Thus, the –OH group present in the RHA network

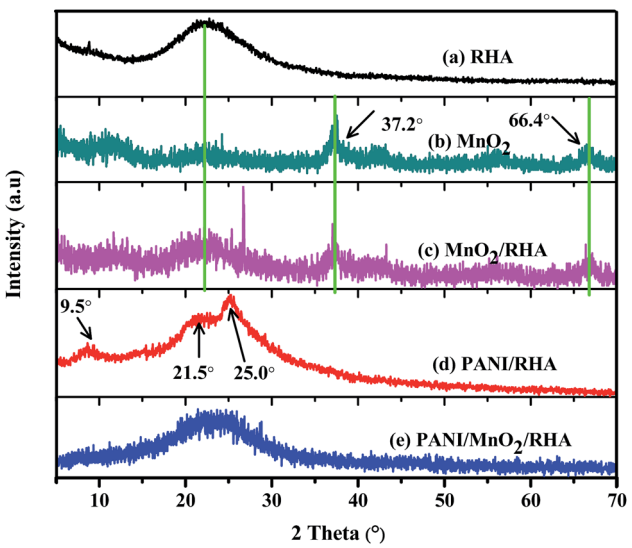

Fig. 6 XRD profile of (a) RHA, (b) MnO_2, (c) MnO_2/RHA, (d) PANI/RHA and (e) PANI/MnO_2/RHA nanocomposites.

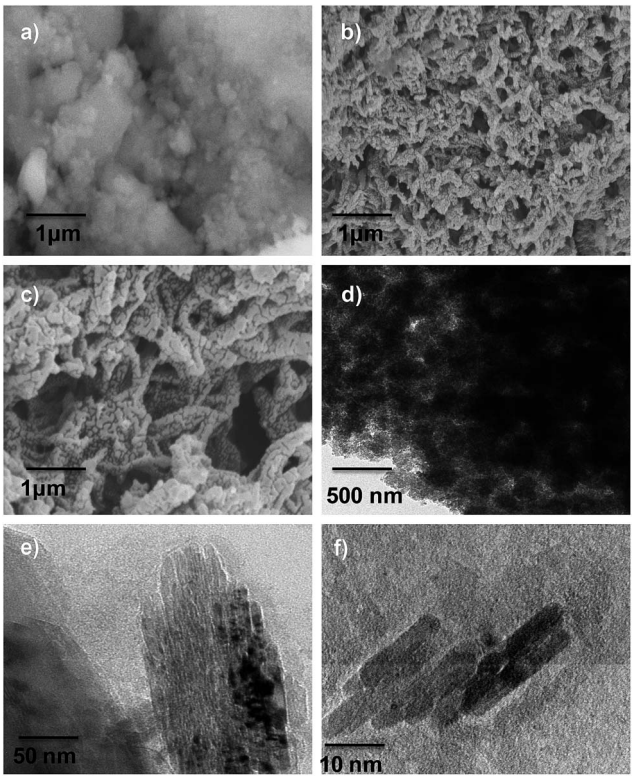

Fig. 7 SEM micrograph of (a) RHA, (b) PANI/RHA and (c) PANI/MnO_2/RHA nanocomposites; TEM micrograph of (d) PANI/RHA and (e–f) PANI/MnO_2/RHA nanocomposites.

also acts as an anchor site for the Mn^{4+} ion. This phenomenon is well supported in Fig. 7e and f, which show homogeneous nucleation of MnO_2 in RHA and PANI grafting.[56] The composition of the PANI/RHA and PANI/MnO_2/RHA obtained from EDAX studies are presented in supporting information (Fig. S2a and b) and Table S3.†

Fig. 8a presents the cyclic voltammograms (CV) of RHA, PANI/RHA and PANI/MnO_2/RHA at 30 mV scan rate in 0.5 M Na_2SO_4 electrolyte from −0.2 to 0.6 V potential window. The formation of a rectangular curve without any redox behaviors clearly illustrates that the neat RHA, PANI/RHA and PANI/MnO_2/RHA demonstrates clear capacitance behavior. Among the nanocomposites, a greater Faradic current response was obtained with PANI/MnO_2/RHA. Due to the effective utilization of both doped MnO_2 with the conductive PANI layer of PANI/MnO_2/RHA, a larger increase in the Faradic performance with fast and reversible capacitance was achieved. Faradic behavior of the neat rice husk ash may be attributed to the presence of 25 wt% carbon content of lignin in the rice husk ash, which was obtained from the thermal treatment of rice husk and supported by the EDAX study of RHA (ESI Fig. S1b and Table S3†). However, PANI-grafted RHA exhibits higher current response with a larger rectangular area due to the enhanced conductance of the PANI/RHA. This enhanced Faradic behavior of PANI/RHA may be attributed to the presence of PANI with a fibrous morphology layer on the RHA surface, which offers a high

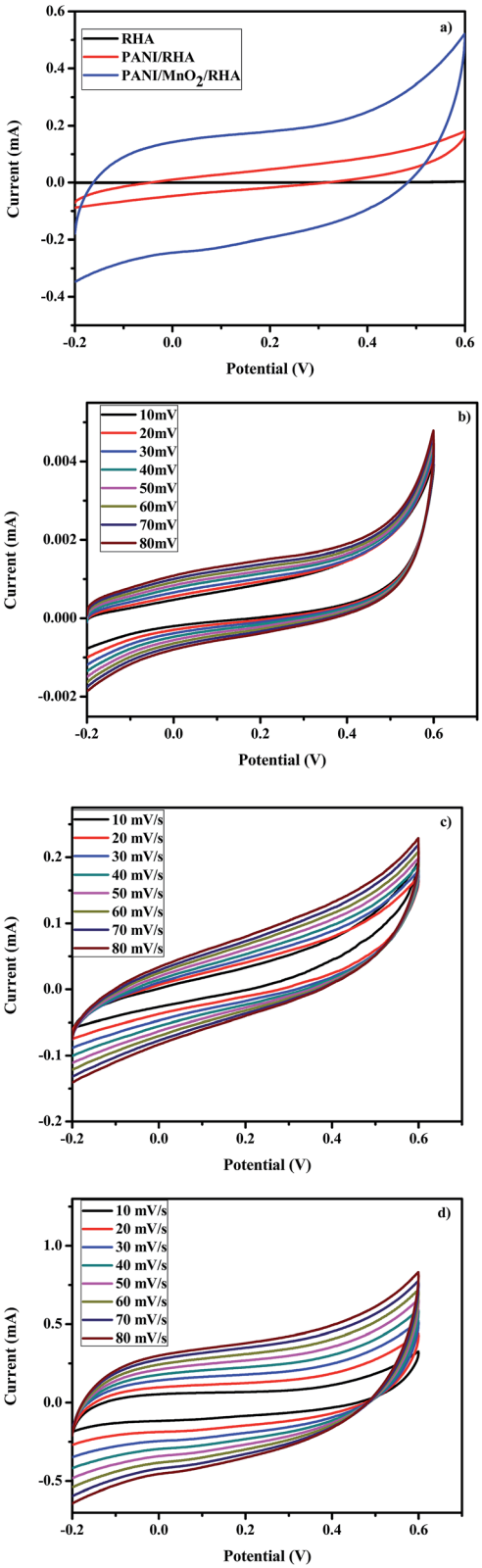

Fig. 8 (a) Cyclic voltammogram (CV) curves of RHA, PANI/RHA and PANI/MnO_2/RHA nanocomposites at 30 mV scan rate. (b–d) Cyclic voltammograms (CV) of RHA, PANI/RHA and PANI/MnO_2/RHA nanocomposites at different scan rates in 0.5 M Na_2SO_4 electrolyte from −0.2 to 0.6 V potential windows.

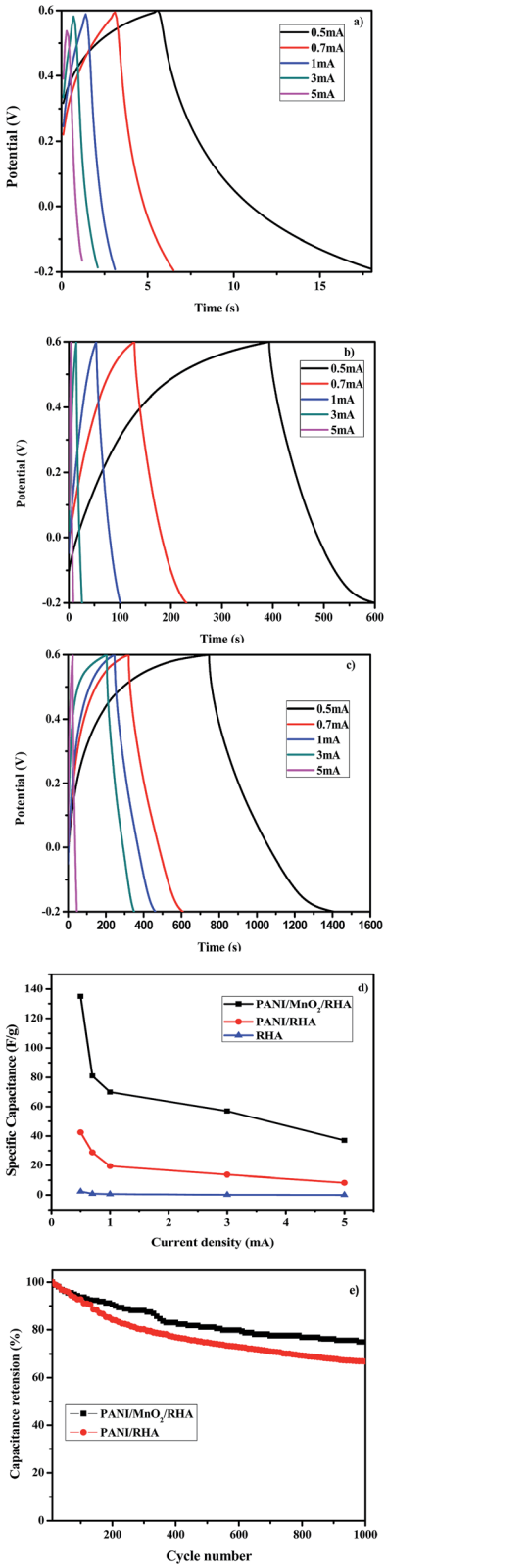

Fig. 9 Charge–discharge curve of (a) RHA, (b) PANI/RHA and (c) PANI/MnO_2/RHA at current densities of 0.5–3 mA g^{-1}. (d) Specific capacitance as a function of different current densities of RHA, PANI/RHA and PANI/MnO_2/RHA. (e) Specific capacitance *versus* cycling number at 0.5 mA g^{-1} of the PANI/RHA and PANI/MnO_2/RHA nanocomposites.

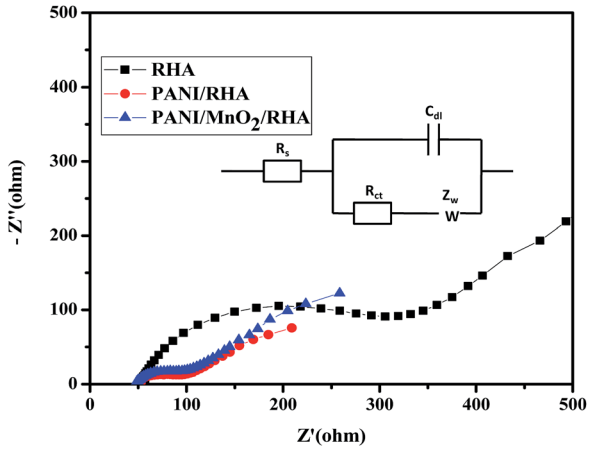

Fig. 10 Nyquist impedance spectra of RHA, PANI/RHA and PANI/MnO_2/RHA.

Table 1 Charge-transfer resistance of the different electrode and electrolyte interfaces

Electrode	R_e (ohm)	C_{dl} (F)	R_{ct} (ohm)	Z_w (ohm)
RHA	51.32	1.74×10^{-6}	189.30	0.00065
PANI/RHA	56.74	1.00×10^{-6}	36.32	0.00002
PANI/MnO_2/RHA	51.51	2.15×10^{-6}	34.46	0.00004

surface area and thus facilitates a larger electrode/electrolyte interface with enhanced electron transfer through the conductive network.[2,57] Further, Fig. 8b–d illustrates a uniform rectangular shape even at higher scan rates, which suggests the characteristic behavior of double-layer capacitance.

Further, evaluations of capacitance behavior with galvanostatic charge–discharge study at 0.5–5 mA g^{-1} are illustrated in Fig. 9a–c for the composites of RHA, PANI/RHA and PANI/MnO_2/RHA. It is noteworthy that the PANI/MnO_2/RHA and PANI/RHA nanocomposites tend to show 135 F g^{-1} and 42.5 F g^{-1} specific capacitance, respectively, at a low current density of 0.5 mA g^{-1}. The nanocomposites developed with PANI and MnO_2-doped PANI grafted are found to show 17- and 54-fold higher capacitance than that of rice husk ash, whose capacitance is 2.5 F g^{-1}. The large surface area with mesoporous morphology offered by MnO_2 and the highly conductive polyaniline network jointly provide better conducting pathways for both ionic (Na^+) and electronic (e^-) transportation during the rapid charge/discharge process and facilitate the high specific capacitance of PANI/MnO_2/RHA nanocomposites.[35,57–59]

Further, the carbon present in the silica-rich rice husk ash acts as a binding material in addition to the Faradic behavior. Thus, it inhibits the addition of active materials like active carbon in electrode preparation. The resulting rate capabilities of the developed composites are compared in Fig. 9d. For the PANI/MnO_2/RHA nanocomposites, the specific capacitance at the current densities of 0.5, 0.7, 1.0, and 3.0 mA g^{-1} were found to be 135, 89, 70, and 57 F g^{-1}, respectively. However, when the current rate was raised to 0.7, 1.0, and 3.0 mA g^{-1}, the resulting capacitance retention was found to be 70.6, 53.8, and 43.8%, respectively. However, the RHA and PANI/RHA tend to show only 0.1% and 32.2% retention, respectively, when the current density is raised to 3.0 mA g^{-1} from 0.5 mA g^{-1}. Thus, the PANI/MnO_2/RHA sample retains maximum rate capability. The long-term cycling stability of the PANI/MnO_2/RHA and PANI/RHA nanocomposites were also studied by charge–discharge measurements at a current density of 0.5 mA g^{-1} for 1000 cycles, and results are illustrated in Fig. 9e. The nanocomposite PANI/MnO_2/RHA exhibited a high electrochemical stability with 74.5% capacitance retention, whereas the PANI/RHA shows only 66.4% retention. The improved cycling stability of PANI/MnO_2/RHA may be due to the large surface area with mesopores. The presence of RHA Si core with doped MnO_2 offers a more stable solid skeleton to interlink the polyaniline skeleton, and in turn, the grafted PANI protects the MnO_2 from dissolving in the electrolyte.[2,60,61] The lower capacitance of PANI/RHA is probably due to the degradation of the polyaniline skeleton.

Electrochemical impedance spectra in the form of Nyquist plots of RHA, PANI/RHA and PANI/MnO_2/RHA are presented in Fig. 10. The electrochemical behavior at the interface between the electrode and electrolyte is well understood from the semicircle in the high frequency region and a 45° capacitive slope in the low frequency region.

Components including electrolyte resistance, intrinsic resistance of active material and contact resistance constitute the observed semicircle behavior. The charge-transfer resistances of the different electrode and electrolyte interfaces are presented in Table 1. From the results of R_{ct}, the PANI/MnO_2/RHA system shows the least charge transfer resistance among the three electrode materials. Due to the presence of capacitive materials and the conductive network both in macro and mesoscopic levels of RHA, the PANI/MnO_2/RHA nanocomposites delivered the larger Faradic response.[62,63]

Conclusion

The renewable bio-source RHA was used in an energy storage system without any further chemical activation. Grafting of polyaniline over the rice husk ash surface was confirmed by ^{29}Si Cp-mas, XPS and EDAX. In addition, doping of MnO_2 was also confirmed by XPS survey. Electrochemical studies of the PANI/MnO_2/RHA hybrid nanocomposite show a higher value of capacitance at 135 F g^{-1}, along with superior stability and long-term reversibility. Thus, the renewable bio-source RHA can be used as an anode material for the fabrication of super capacitors, which can be utilized at large scale and with competitive cost in the future.

Acknowledgements

The authors thank BRNS, G. no.: 2012/37C/9/BRNS, Mumbai, Govt. of India, for the financial support and also thank Dr Manmohan Kumar, Senior Scientific Officer, BARC, Mumbai.The authors thank Dr M.R. Vengatesan, Sungkyunkwan University, Suwon, South Korea, Dr S. Devaraju, Pusan National University, Busan, 609-735, South Korea, and Dr Padmanaban, Dept. of Physics, Anna University for their support.

References

1 M. Biswal, A. Banerjee, M. Deo and S. J. Ogale, *Energy Environ. Sci.*, 2013, **6**, 1249.
2 M. Kim, S. Cho, J. Song, S. Son and J. Jang, *ACS Appl. Mater. Interfaces*, 2012, **4**, 4603.
3 W. T. Deng, X. B. Ji, Q. Y. Chen and C. E. Banks, *RSC Adv.*, 2011, **1**, 1171.
4 C. D. Lokhande, D. P. Dubal and O. S. Joo, *Curr. Appl. Phys.*, 2011, **11**, 255.
5 Z. Algharaibeh, X. R. Liu and P. G. Pickup, *J. Power Sources*, 2009, **187**, 640.
6 Y. H. Lin, T. Y. Wei, H. C. Chien and S. Y. Lu, *Adv. Energy Mater.*, 2011, **1**, 901.
7 H. Jiang, T. Zhao, C. Z. Li and J. Ma, *J. Mater. Chem.*, 2011, **21**, 3818.
8 M. Hasan, M. Jamal and K. M. Razeeb, *Electrochim. Acta*, 2012, **60**, 193.
9 H. Shi, *Electrochim. Acta*, 1996, **41**, 1633.
10 D. Qu and H. Shi, *J. Power Sources*, 1998, **74**, 99.
11 Y. Guo, J. Qi, Y. Jiang, S. Yang, Z. Wang and H. Xu, *Mater. Chem. Phys.*, 2003, **80**, 704.
12 N. Bagheri and J. Abedi, *Chem. Eng. Res. Des.*, 2009, **87**, 1059.
13 M. T. Tsay and F. W. Chang, *Appl. Catal., A*, 2000, **203**, 15.
14 M. Ahmaruzzaman and V. K. Gupta, *Ind. Eng. Chem. Res.*, 2011, **50**, 13589.
15 M. Y. Ahmad Fuad, Z. Ismail, M. S. Mansor, Z. A. Mohd Ishak and A. K. Mohd Omar, *Polym. J.*, 1995, **27**, 1002.
16 Y. C. Y. Zhu, Z. Wang, Y. Li, L. Wang, L. Ding, X. Gao, Y. Ma and Y. Guo, *Adv. Colloid Interface Sci.*, 2011, **163**, 39.
17 X. He, P. Ling, M. Yu, X. Wang, X. Zhang and M. Zheng, *Electrochim. Acta*, 2013, **105**, 635.
18 L. John Kennedy, J. Judith Vijaya and G. Sekaran, *Ind. Eng. Chem. Res.*, 2004, **43**, 1832.
19 N. Liu, K. Huo, M. T. McDowell, J. Zhao and Y. Cui, *Sci. Rep.*, 2013, **3**, 1.
20 L. Wang, Z. Schneppb and M. M. Titirici, *J. Mater. Chem. A.*, 2013, **1**, 5269.
21 S. Kumagai, M. Sato and D. Tashima, *Electrochim. Acta*, 2013, **114**, 617.
22 X. He, P. Ling, M. Yu, X. Wang, X. Zhang and M. Zheng, *Electrochim. Acta*, 2013, **105**, 635.
23 A. Imyim and E. Prapalimrungsi, *J. Hazard. Mater.*, 2010, **184**, 775.
24 M. Ghorbani and H. Eisazadeh, *Composites, Part B*, 2013, **45**, 1.
25 M. Ghorbani and H. Eisazadeh, *Synth. Met.*, 2012, **162**, 527.
26 M. Ghorbani, M. S. Lashkenari and H. Eisazadeh, *Synth. Met.*, 2011, **161**, 1430.
27 M. Ghorbani, H. Eisazadeh and A. A. Ghoreyshi, *Iran. J. Energy Environ.*, 2012, **3**, 83–88.
28 J. Han, L. Li, P. Fang and R. Guo, *J. Phys. Chem. C*, 2012, **116**, 15900.
29 J. C. C. Freitas, F. G. Emmerich and T. J. Bonagamba, *Chem. Mater.*, 2000, **12**, 711.
30 F. Adam, H. Osman and K. M. Hello, *J. Colloid Interface Sci.*, 2009, **331**, 143–147.
31 X. Zhang, N. Zhao, W. Wei and Y. Sun, *Catal. Today*, 2006, **115**, 102.
32 Y. Z. Wang, Y. C. Hsu, R. R. Wu and H. M. Kao, *Synth. Met.*, 2003, **132**, 151.
33 Z. D. Zujovic, M. G. Nikoladis, P. A. Kilmartin, J. T. Sejdic, R. P. Cooney and G. A. Bowmaker, *Appl. Magn. Reson.*, 2005, **28**, 123.
34 S. Kaplan, E. M. Conwell, A. F. Richter and A. G. MacDiarmid, *J. Am. Chem. Soc.*, 1988, **110**, 7647.
35 K. S. Kim and S. J. Park, *J. Solid State Electrochem.*, 2012, **16**, 2751.
36 A. J. Schwanke, C. W. Lopes and S. B. C. Pergher, *Mater. Sci. Appl.*, 2013, **4**, 468.
37 S. Karthikeyan and G. Sekaran, *Phys. Chem. Chem. Phys.*, 2014, **16**, 3924.
38 J. Kim, H. Ju, A. I. Inamdar, Y. Jo, J. Han, H. Kim and H. Im, *Energy*, 2014, **70**, 473.
39 S. Hassan, M. Suzuki, S. Mori and A. A. El-Moneim, *RSC Adv.*, 2014, **4**, 20479.
40 A. Sumboja, C. Y. Foo, J. Yan, C. Yan, R. K. Gupta and P. S. Lee, *J. Mater. Chem.*, 2012, **22**, 23921.
41 W. Ni, D. Wang, Z. Huang, J. Zhao and G. Cui, *Mater. Chem. Phys.*, 2010, **124**, 1151.
42 G. Han, Y. Liu, L. Zhang, E. Kan, S. Zhang, J. Tan and W. Tang, *Sci. Rep.*, 2014, **4**, 4824.
43 A. Imyin and E. Prapalimrungsi, *J. Hazard. Mater.*, 2010, **184**, 775.
44 Y. Hou, Y. Cheng, T. Hobson and J. Liu, *Nano Lett.*, 2010, **10**, 2727.
45 S. J. Bao, B. L. He, Y. Y. Liang, W. J. Zhou and H. L. Li, *Mater. Sci. Eng., A*, 2005, **397**, 305.
46 X. Yan, Z. Tai, J. Chen and Q. Xue, *Nanoscale*, 2011, **3**, 212.
47 K. Zhang, L. L. Zhang, X. S. Zhao and J. Wu, *Chem. Mater.*, 2010, **22**, 1392.
48 K. Lee, S. Cho, S. H. Park, A. J. Heeger, C. W. Lee and S. H. Lee, *Nature*, 2006, **441**, 65.
49 B. H. Lee, S. H. Park, H. Back and K. Lee, *Adv. Funct. Mater.*, 2011, **21**, 487.
50 B. Mu, W. Zhang, S. Shao and A. Wang, *Phys. Chem. Chem. Phys.*, 2014, **16**, 787.
51 A. H. Gemeay, I. A. Mansour, R. G. El-Sharkawy and A. B. Zaki, *Eur. Polym. J.*, 2005, **41**, 2575.
52 P. Tang, L. Han and L. Zhang, *ACS Appl. Mater. Interfaces*, 2014, **6**, 10506.
53 W. Zou, W. Wang, B. He, M. L. Sun and Y. Sheng Yin, *J. Power Sources*, 2010, **195**, 7489.
54 M. Ghorbani, M. S. Lashkenari and H. Eisazadeh, *Synth. Met.*, 2011, **161**, 1430.
55 S. A. Iranagh, L. Eskandarian and R. Mohammadi, *Synth. Met.*, 2013, **172**, 49.
56 D. R. Rolison, J. W. Long, J. C. Lytle, A. E. Fischer, C. P. Rhodes, T. M. McEvoy, M. E. Bourga and A. M. Lubers, *Chem. Soc. Rev.*, 2009, **38**, 226.
57 J. Xu, K. Wang, S. Z. Zu, B. H. Han and Z. Wei, *ACS Nano*, 2010, **4**, 5019.

58 P. Lv, Y. Y. Feng, Y. Li and W. Feng, *J. Power Sources*, 2012, **220**, 160.
59 Y. Liu, D. Yan, R. Zhuo, S. Li, Z. Wu, J. Wang, P. Ren, P. Yan and Z. geng, *J. Power Sources*, 2013, **242**, 78.
60 H. Jiang, Y. Dai, Y. Hu, W. Chen and C. Li, *ACS Sustainable Chem. Eng.*, 2014, **2**, 70.
61 J. G. Wang, Y. Yang, Z. Huang and F. Kang, *Electrochim. Acta*, 2014, **130**, 642.
62 L. Chen, Z. Song, G. Liu, J. Qiu, C. Yu, J. Qin, M. Lin, F. Tian and W. Liu, *J. Phys. Chem. Solids*, 2013, **74**, 360.
63 P. A. Basnayaka, M. K. Ram, E. K. Stefanakos and A. Kumar, *Electrochim. Acta*, 2013, **92**, 376.